Engineered Science
DOI : https://dx.doi.org/10.30919/es928

On the Development of a Passive Shape Memory Alloy- Based Cooling System – Part II: Design Justification

Aniello Riccio,[1] Andrea Sellitto,[1,*] Antonio Caraviello,[2] Ugo Riccio,[3] Antonio Torluccio,[3] Luca Pacini[3] and Rouven Mohr[3]

Abstract

The use of shape memory alloy (SMA)-based actuators is more and more increasing, thanks to the potential benefits in terms of actuation power/weight ratio and weight reduction, if compared to traditional electromechanical actuators. In this paper, part of the Research and Development activities finalised to the prototyping of a SMA-based cooling system device for automotive applications is introduced. The SMA actuator is passively controlled by the temperature reached in the engine compartment. Indeed, the increase of temperature beyond a predetermined threshold, triggers, by means of the SMA-based actuator, a set of cooling flaps which dissipate the heat accumulated in the engine compartment. Actually, the performed extensive development activity has been split into two parts which are presented in two papers. The present paper focuses on part II, dealing with detailed finite element analyses and optimization, aimed to the numerical justification of the design; while, part I, focused on Design, Manufacturing and Testing of the proposed passive cooling system, is presented in a parallel paper. The evolution of the geometrical configurations of the SMA-based cooling system device, throughout the design and optimization phases, is shown. Finally, results from detailed finite element analyses, performed on the final executive design configuration and aimed to verify the fulfilment of SMA device operating requirements, are introduced and commented to justify the choices made in the frame of the design phases.

Keywords: FEM; Passive cooling system; SMA; Actuator.
Received: 20 January 2023; Revised: 09 June 2023; Accepted: 15 June 2023.
Article type: Research article.

1. Introduction

The interest towards shape memory alloys (SMA)-based applications is unquestionably increasing in the recent years, thanks to their benefits in terms of actuation power/weight ratio and weight reduction. Among the others, one of the most promising field of application is the adaptive aerodynamic, where SMA-based smart structures can be used to autonomously modify the shape of the structure to reach the best aerodynamic performance in every condition.[1-8]

Shape memory alloys (SMA), when subjected to the application of a load, are able to recover their original shape if heated above a predefined threshold temperature.[9-11] This property, called shape memory effect, is due to a phase transition of the internal crystal lattice. The memory effect, due to the high actuation power/weight ratio, makes SMA particularly attractive for applications where actuators are involved. Indeed, the SMAs are characterized by two phases: the martensitic phase, which is stable at low temperature and high stress, and the austenitic phase, which is stable at high temperature and low stress.[12-14] The phase transition from austenite to martensite is known in the literature as forward transformation, while the transformation martensite to austenite is named reverse transformation.[15] In this context, the following characteristic transformation temperatures can be identified: Ms – martensite start (below this temperature, the material starts the transition into martensite phase), Mf – martensite finish (below this temperature, the material has completed the transition into martensite phase), As – austenite start (above this temperature, the material starts the transition into austenite phase, Af – austenite finish (above this temperature, the material has completed the transition into

[1] *University of Campania "Luigi Vanvitelli", Department of Engineering, via Roma 29, Aversa (CE), 81031, Italy.*
[2] *Sòphia High Tech, via Romani 228, Sant'Anastasia (NA), 80048, Italy.*
[3] *Automobili Lamborghini S.p.A., Via Modena 12, Sant'Agata Bolognese (BO), 40019, Italy.*
**Email:* andrea.sellitto@unicampania.it (A. Sellitto)

© Engineered Science Publisher LLC 2023

austenite phase).

According to the shape memory effect, SMA actuators are able to develop recovery forces, moments, or displacements by imposing an initial deformation and, then, by heating them above the phase transformation temperature.

During the last decades, many SMA-based applications have been proposed in very different fields, from Biomedics.[16-18] to industry.[19-22] encouraging the development of new solutions able to guarantee relevant improvement in actuator design. Among the others, an interesting design solution commonly found in literature is based on the assembly of two SMA elements working against each other, which results in the so-called antagonistic actuator.

Several studies can be found in the literature focused on the simulation of SMA-based devices. A deployment mechanism of a composite satellite antenna structure, actuated by SMA hinges, has been studied in Ref. [23], where the shape memory effect has been analysed by using finite element modelling. In Ref. [24], finite element analyses have been used to investigate the response of smart structures based on shape memory alloys and piezoceramics materials.

The present work is focused on the numerical design verification of a SMA-based cooling system device. The investigated device is aimed to the control of the rear flaps of the Rear-Bonnet of the Lamborghini Aventador S as test case. The load triggering the flaps is provided by the SMA springs, which are activated by thermal convection when the threshold temperature for SMA phase transformation is reached in the engine compartment. Due to this characteristic, the device can be considered passively activated independently from the vehicle electronic control systems. The absence of electromechanical actuation allows the reduction of the vehicle weight and of the engine cooling system complexity.

Design verification by Finite Element analyses is a well-consolidated practice able to reduce the overall design time and cost and increase the structural safety. The structural design of auxiliary device for installation of large vertical equipment and its verification by using finite element approach is studied in Ref. [25], to determine its compliance to the operational requirements. In Ref. [26], the design of soft magnetic composite devices is investigated, and their optimization is presented by using simplified numerical FE models.

In this work, the DMAIC (Define, Measure, Analyse, Improve, Control) approach, summarized in the flowchart of Fig. 1, has been considered to guarantee effective results. Actually Fig. 1, introduces the activities performed to develop the SMA-based cooling system device.

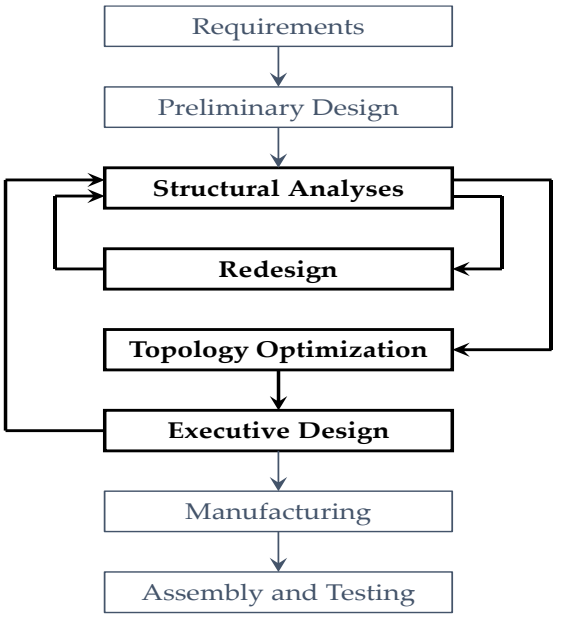

Fig. 1 Activities flowchart.

This paper, describing the part II of the performed activities, has been arranged according to the bold test boxes of the flowchart in Fig. 1 Structural analyses, Redesign, Topology optimization and Executive Design verification. Actually, the Requirements, the Preliminary Design, the Executive Design, the Manufacturing, the Assembly and the Testing activities, which provide the baseline activities for the developed design, are introduced in the part I paper.[27] In the frame of this work, the numerical analyses are focused to demonstrate the effectiveness and robustness of the actuator system, respect to the requirements introduced in the part I paper. Therefore, the compatibility with the Aventador has been investigated experimentally, as discussed in the part I manuscript.

In section 2 the intermediate SMA-based cooling system device configurations, leading to the final executive design are briefly introduced and described. Then, in section 3 the final executive design is presented, and the numerical results from detailed finite element analyses, aimed to the verification of the compliance with the device operative requirements, are presented and assessed.

2. SMA-based cooling system device configuration evolution

As already remarked, the proposed SMA-based Cooling System Device is aimed to lower the temperature inside the engine compartment, by opening flaps on the rear-bonnet of the car. The operating loading conditions provided by the customer are detailed in Ref. [27]. Some relevant information on the requirements are briefly recalled in the present paper. In particular, the passive cooling system must guarantee a 60° flap rotation as soon as the temperature in the engine

© Engineered Science Publisher LLC 2023

compartment reaches the temperature target $T_{activation}$. The system must guarantee operations on flaps when the vehicle is stationary; furthermore, the system must ensure that the flaps remain in the opened or closed position (depending on temperature in the engine compartment), when the vehicle is in motion up to a 350 km/h speed. Therefore, the system must be dimensioned to guarantee the opened or closed flaps condition when the aerodynamic loads generated by the movement of the vehicle are applied. Hence, two loading conditions can be preliminary introduced:

Closed configuration: in this case the flaps are in closed position and the maximum suction load equal to 13 N is applied on all flaps.

Open configuration: in this case the flaps are 60° rotated and the maximum compression load equal to 19 N is considered.

As final requirement, the passive cooling system should not be subjected to any permanent deformation and/or breakage due to the operative loads.

The development of the final executive design configuration is the result of a design loop process. This process involved the development of several intermediated configurations. In this section, a brief description of each developed configuration is presented, including the technical motivations related to the configurations' development. All the subcomponents of the proposed SMA-based Cooling System Device, except the sliding guides and rails (which are commercial products) and the small parts (screws, pins, bearings), are custom.

In Fig. 2, the evolution across the different configurations, from the first preliminary configuration up to the executive design, is schematically introduced.

According to the preliminary design configuration, the developed SMA-based Cooling System Device is made of different components. The main components are reported in Fig. 3 and, hereafter, briefly described.

SMA Spring Assembly: The SMA Spring Assembly is the components' group which contains the SMA and bias springs. It is the part directly exposed to the heat generated by the engine, and the one which generates the load needed to actuate the device. The load is triggered by the phase transition on the SMA components induced by the temperature increase in the engine compartment.

Crankcase: The crankcase is the component devoted to enclose the internal mechanism of the device and to connect its different parts. The crankcase is closed on the side exposed to the engine and it is directly connected to the SMA spring assembly.

Joints: The joints system is the internal mechanism aimed to transfer the linear displacement provided by the SMA spring assembly into a linear movement in the normal direction with respect to the rotating axes of the flaps. As a requirement, the joints system must ensure the simultaneous movement of the flaps located on the left and right side of the device.

Slide and rail: Slides and rails (one per side) are used to guide the linear movement induced by the spring assembly in the normal direction with respect to the rotation axes of the flaps. The rails are integrated within the crankcase, while the slides are connected to the joint system.

Rack: the racks (one per side) are used to transfer the displacement to the gear rods connected to the flaps support.

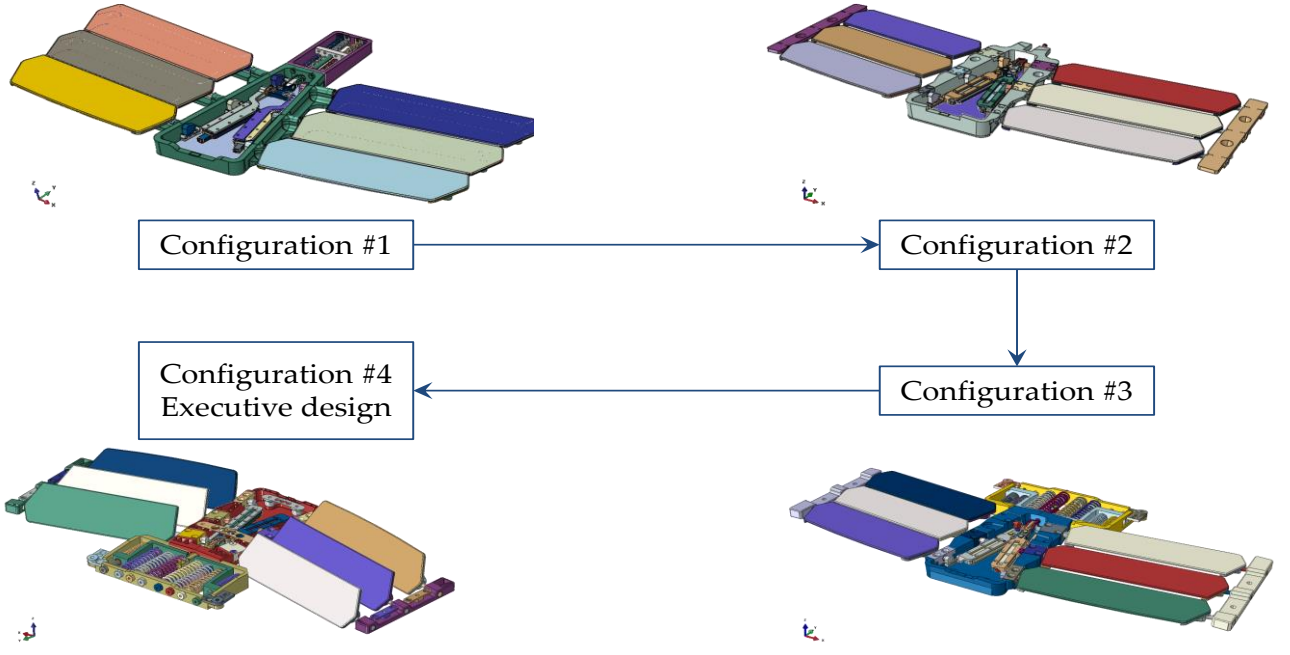

Fig. 2 Evolution of the developed configurations.

© Engineered Science Publisher LLC 2023

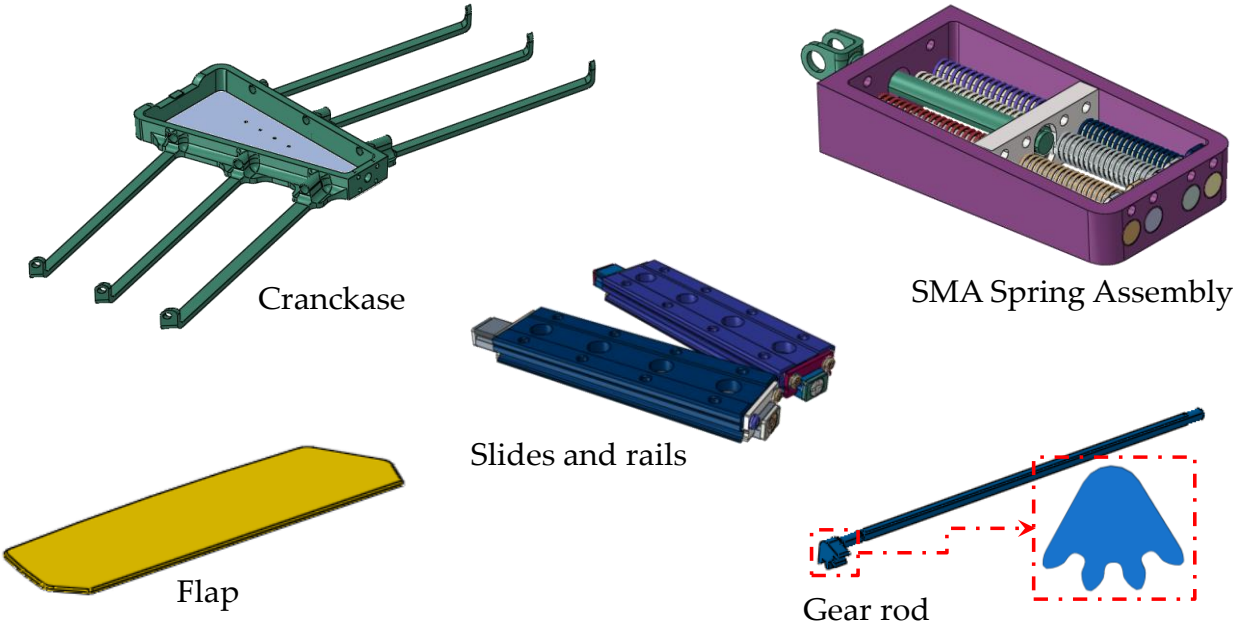

Fig. 3 Passive cooling system main components (Configuration #1).

Each rack consists of three sets of teeth, each consisting of five (configuration #1 and configuration #2) or nine (configuration #3 and configuration #4) teeth.

Gear rod: the gear rods (six, one per flap) are connected to the flap brackets. The linear displacement of the rack induces the rotation of the flaps by means of the gear rods.

Flap bracket: The flap brackets (six, one per flap) are used to support the flaps, acting as an interface between the passive cooling system and the flap (supplied by the customer) themselves. The shape and size of this component is prescribed by the specific flaps they must support.

Side support (from Configuration #2): the two external supports (one per side) are used as an additional constraint for the flap brackets, to support the flaps and keep them in position during the actuation. These components are not included in configuration #1, since, for this configuration, they are integrated into the Crankcase.

Flap: The six flaps are not an active part of this study, since they are directly supplied by the customer. However, they play an important role on the SMA-based Cooling System Device dimensioning because the aerodynamic loads, which results in the internal load acting on the device, are applied on their surfaces.

Three different materials have been considered for the design of the SMA-based Cooling System Device: aluminium alloy, steel, and fabric CFRP (Carbon fibre reinforced plastic). In particular, aluminium alloy has been used for the external components, while the internal components (the ones devoted to the load transfer) are made of steel. CFRP is only applied to the flaps, since they are part of the rear bonnet and have to be perfectly integrated with it. The mechanical properties of the different material systems are reported in Table 1.

Table 1. Mechanical properties of the material systems.

	Aluminium Alloy	Steel		CFRP
Young Modulus E [MPa]	72500	210000	Young Modulus $E_{11} = E_{22}$ [MPa]	52000
Poisson's ratio ν	0.3	0.3	Young Modulus E_{33} [MPa]	8000
Yield Stress σ_y [MPa]	210	350	Poisson's ratio ν_{12}	0.3
Ultimate Stress σ_r [MPa]	280	430	Shear Modulus G_{12} [MPa]	13000
Density ρ [g/cm^3]	2.6	7.8	Shear Modulus $G_{13} = G_{23}$ [MPa]	5000

To verify each configuration, different numerical analyses have been performed. However, for the sake of brevity, these analyses are only briefly listed: a detailed discussion of the results is reported only for the final executive design (configuration #4).

The numerical analyses carried out on the configuration #1, shown in Fig. 4, are herein described:

© Engineered Science Publisher LLC 2023

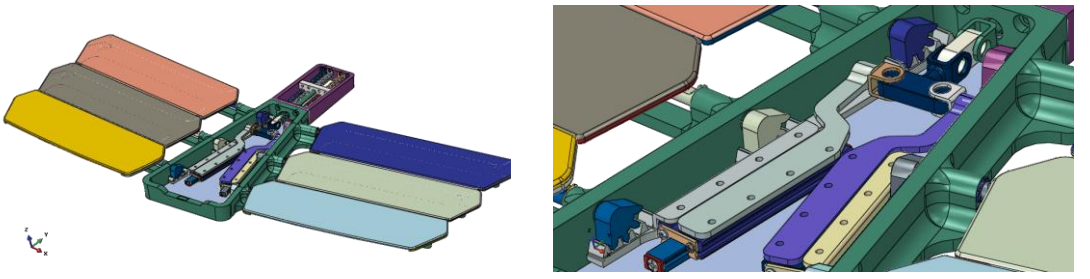

a) b)

Fig. 4 (a) configuration #1 assembly; (b) details on Crankcase and joints.

Analysis 1 – Kinematic verification: this analysis was aimed to verify the kinematics of the device and to evaluate the resulting stress field. In this test case, the aerodynamic load has been neglected.

Analysis 2 – Verification of the maximum loading condition in the opened flaps configuration: this analysis was aimed to verify the stress field and the deformations of the system when subjected to the maximum loading condition, in terms of maximum applied moments on the flaps, and locked joints. This analysis has been performed considering the device in the opened flaps configuration.

The simplification of the Joints system and Rack assembly, because of general manufacturing requirements, led to the definition of configuration #2 which is shown in Fig. 5.

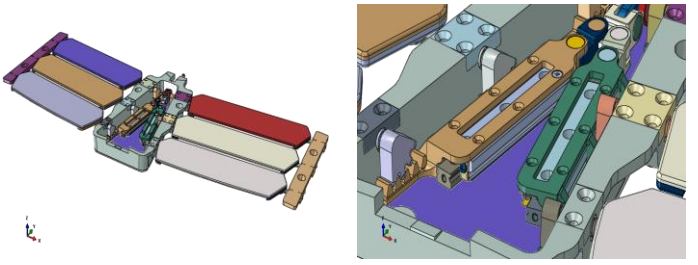

a) b)

Fig. 5 (a) configuration #2; (b) details on crankcase and joints.

The numerical analyses performed on the configuration #2 are herein described:

Analysis 1 – Kinematic motion.

Analysis 2 – Verification of the flap deformation under aerodynamic loading condition: the analysis was aimed to evaluate the deformations of the flaps and their supports due to the maximum aerodynamic load applied as pressure acting on the flaps. The kinematic mechanism is locked in the opened flaps configuration.

Analysis 3 – Verification of the maximum loading condition in the closed flaps configuration: This analysis was aimed to verify the stress field and the deformations of the system when subjected to the maximum loading condition, in terms of maximum applied moments on the flaps, and locked joints. This analysis has been performed considering the device in the closed flaps configuration.

Analysis 4 – Verification of the maximum loading condition in the opened flaps configuration: this analysis was aimed to verify the stress field and the deformations of the system when subjected to the maximum loading condition, in terms of maximum applied moments on the flaps, and locked joints. This analysis has been performed considering the device in the opened flaps configuration.

Configuration #3, shown in Fig. 6, is representative of the final SMA-based Cooling System Device executive design characteristics, including a series of modifications, starting from configuration #2, which arise from technical/manufacturing requirements. In particular, the main changes are related to the spring assembly: following a series of considerations and evaluations related to the operation of the SMAs and to the space available for installation of the device, the maximum stroke has been set to 5 mm. The gearwheels have, therefore, been modified: their diameter has been reduced to achieve a rotation of 60° with 5 mm displacement imposed by the SMAs. Consequently, the design of the teeth for both wheels and racks has been modified as well. A further change concerns the coupling system with the sub-rear-bonnet.

In configuration #3, two small metal flanges have been glued to the sub-rear-bonne to connect the SMA-based Cooling System Device by means of mechanical connections. The following numerical analyses have been performed on the configuration #3 to verify its robustness and the satisfaction of requirements:

- **Analysis 1 – Kinematic motion.**
- **Analysis 2 – Verification of the Flap deformation under aerodynamic loading condition (compression):** the analysis was aimed to evaluate the deformations of the flaps and their supports due to the maximum aerodynamic load applied in compression as pressure acting on the flaps. The kinematic mechanism is locked in the opened flaps configuration.

© Engineered Science Publisher LLC 2023

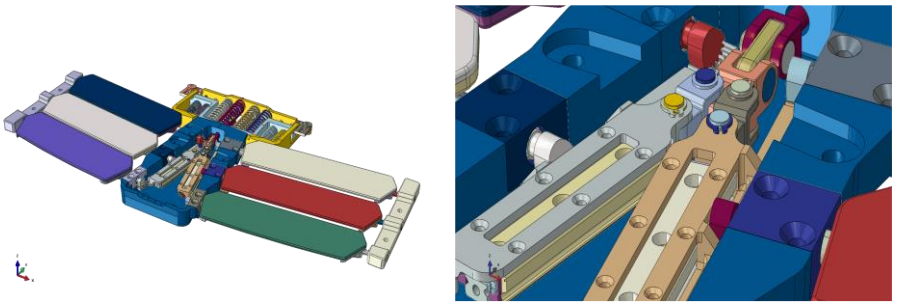

a) b)

Fig. 6 (a) configuration #3; (b) details on Crankcase and joints.

- **Analysis 3 – Verification of the Flap deformation under aerodynamic loading condition (suction):** the analysis was aimed to evaluate the deformations of the flaps and their supports due to the maximum aerodynamic load applied in suction as pressure acting on the flaps. The kinematic mechanism is locked in the closed flaps configuration.
- **Analysis 4 – Verification of the maximum loading condition in the closed flaps configuration:** This analysis was aimed to verify the stress field and the deformations of the system when subjected to the maximum loading condition, in terms of maximum applied moments on the flaps, and locked joints. This analysis has been performed considering the device in the closed flaps configuration.
- **Analysis 5 – Verification of the maximum loading condition in the opened flaps configuration:** this analysis was aimed to verify the stress field and the deformations of the system when subjected to the maximum loading condition, in terms of maximum applied moments on the flaps, and locked joints. This analysis has been performed considering the device in the opened flaps configuration.

The final Executive design (configuration #4) derives from configuration #3. Actually, no substantial change has been made from a functional point of view. Indeed, the final executive design is the result of an optimization analysis performed on configuration #3 and aimed to the reduction of the mass, which is obtained by removing material from low stressed regions. A sketch of configuration #4 (final executive design) geometry is reported in Fig. 7.

Actually, following the verification of the robustness of the design (performed on configuration #3), a structural optimisation has been carried out on components of the SMA-based Cooling System Device, aimed to weight reduction. An extensive optimization activity has been performed on the components produced by additive manufacturing technologies. Indeed, for these components, the more complex geometry, resulting from the optimization procedure, did not result in an increase in production time and costs; on the contrary, less material and smaller sintered volume was needed, resulting in reduced production costs and time. The components subject to the optimisation procedure are the crankcase, the flap supports, and the side supports. The Final geometric configuration of the main components of configuration #4 are shown in Fig. 8.

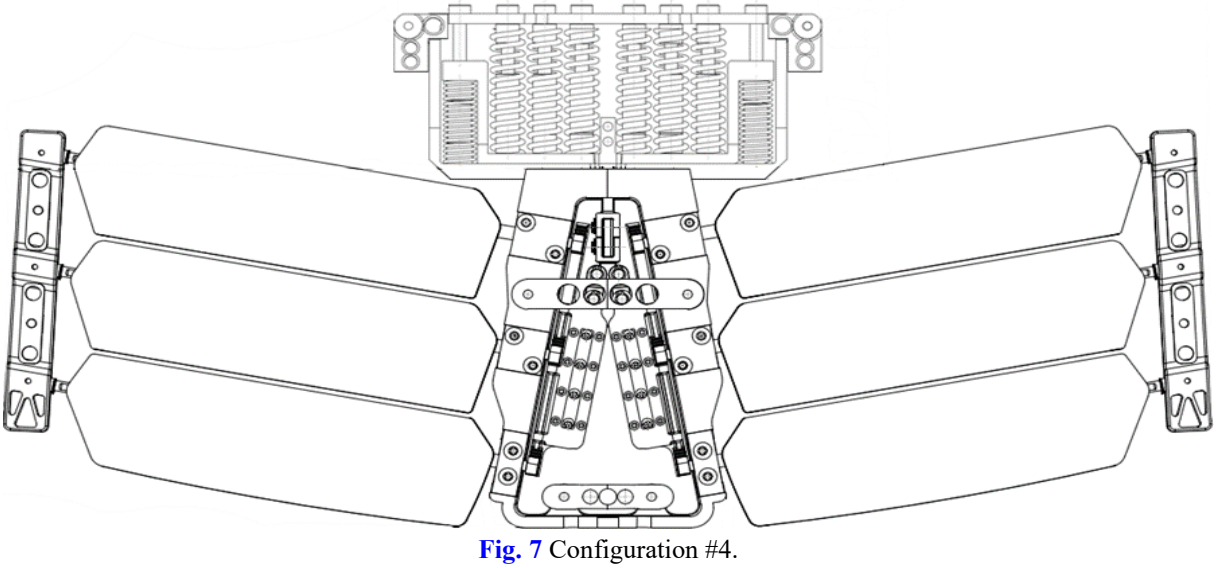

Fig. 7 Configuration #4.

© Engineered Science Publisher LLC 2023

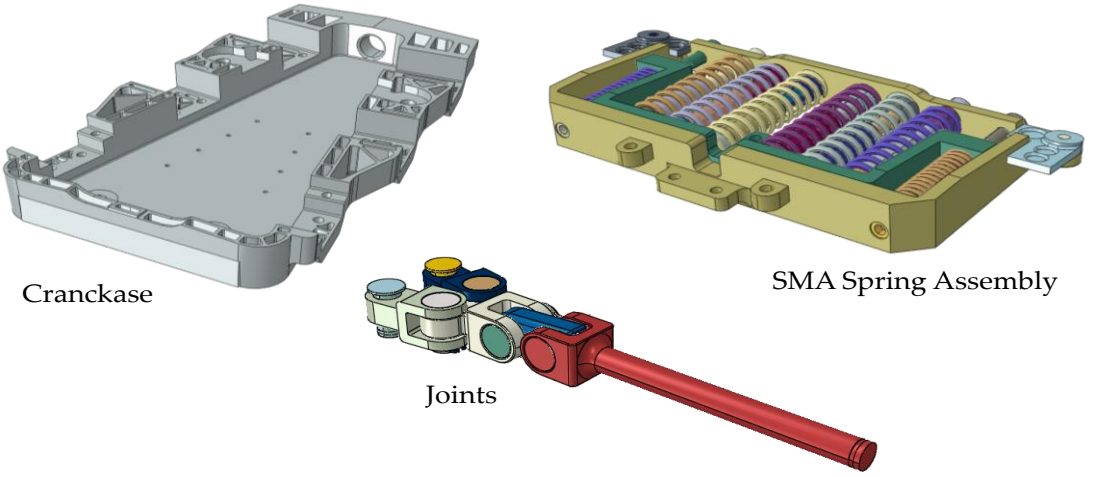

Fig. 8 SMA-based cooling system device main components (configuration #4).

Table 2 reports the reduction in terms of volume and mass of the optimised components of configuration #4 compared to those of configuration #3. In this table, the data refers to all the six flap supports and to the two side supports.

3. SMA-based cooling system device executive design verification

The Finite Element models and Finite Element analyses results aimed to verify the satisfaction of requirements for the final executive design are presented in this section. Considering the geometrical characteristics of the model and the complexity of the simulations, to reduce the computational costs, only one half of the SMA-based Cooling System Device domain has been considered in computations as shown in Fig. 9. Appropriate symmetry boundary conditions have been applied in the adopted FEM environment ABAQUS. The half FE model has been discretized with 301,366 solid elements (C3D8R and C3D4) and 472,761 nodes. The Finite Element Model is introduced in Fig. 10, which shows the material systems associated to the different components of the investigated device. Details of the FE discretization are reported in Fig. 11. Connector elements have been used to simulate the pins connecting joints.

Table 2. Model #3 and Model #4 volume and mass comparisons.

	Flap supports		Side supports		Crankcase	
	Volume [mm^3]	Mass [kg]	Volume [mm^3]	Mass [kg]	Volume [mm^3]	Mass [kg]
Model #3	140,000.0	0.393	46,682.0	0.131	86,826.0	0.243
Model #4	105,836.1	0.296	34,592.0	0.097	64,676.4	0.181
Reduction	24.7 %	24.7 %	25.9 %	25.9 %	25.5 %	25.5 %

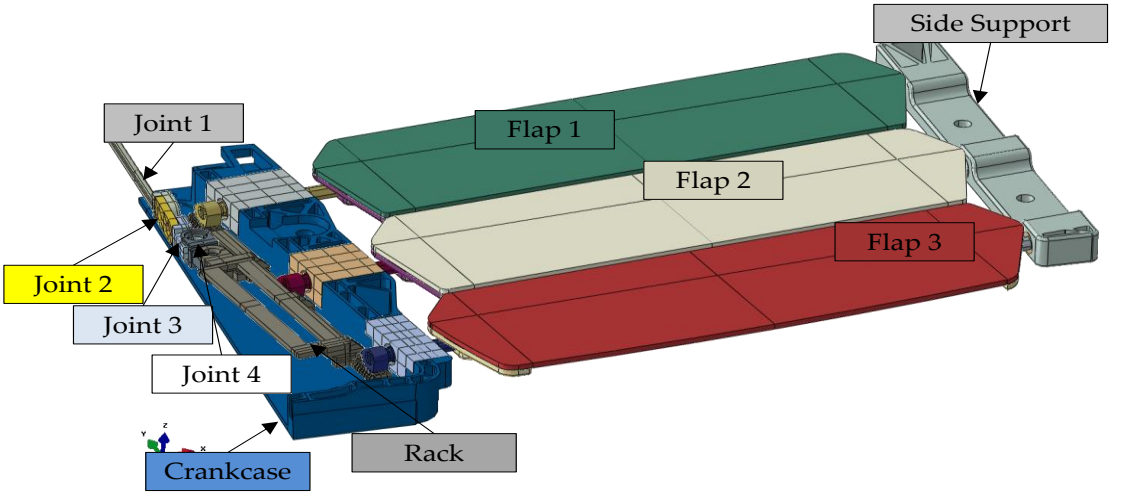

Fig. 9 Investigated domain.

© Engineered Science Publisher LLC 2023

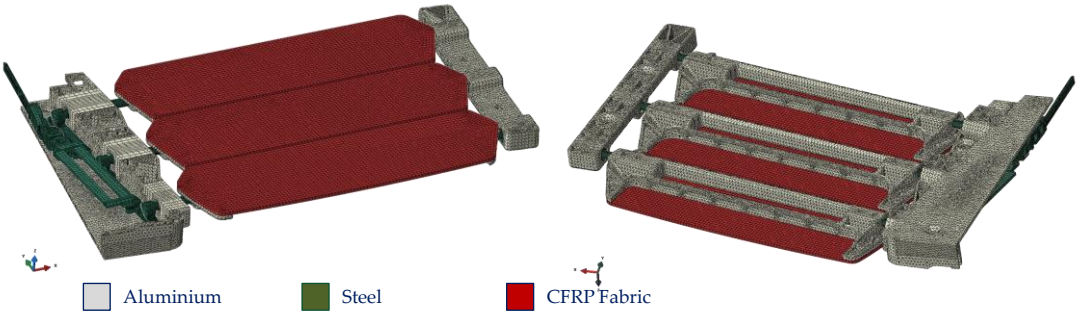

Fig. 10 Finite Element Model and associated material systems.

As for the previously investigated configurations, several verification analyses have been performed for configuration #4 except for kinematics. Actually, kinematics has not been verified for configuration #4, since the variations introduced with respect to configuration #3 do not affect the device from an operational point of view. The following numerical analyses have been performed on the configuration #4 to verify its robustness and the satisfaction of requirements:

- **Analyses 1 – Structural verification of the optimised components:** Some components have been subjected to an optimisation procedure aimed to reduce weight without affecting the structural performance. Therefore, these analyses have been finalised to the verification of each optimized component individually. Hence, four analyses have been carried out one for each optimized component: crankcase (Analysis 1.1), side supports (Analysis 1.2), and flap supports (Analysis 1.3).
- **Analysis 2 – Verification of the maximum loading condition in the closed flaps configuration:** This analysis was aimed to verify the stress field and the deformations of the system when subjected to the maximum loading condition, in terms of maximum applied moments on the flaps, and locked joints. This analysis has been performed considering the device in the closed flaps configuration.
- **Analysis 3 – Verification of the maximum loading condition in the opened flaps configuration:** This analysis was aimed to verify the stress field and the deformations of the system when subjected to the maximum loading condition, in terms of maximum applied moments on the flaps, and locked joints. This analysis has been performed considering the device in the opened flaps configuration.

In the following subsection the numerical results obtained for each verification Analysis are presented and commented.

Analysis 1.1 – Verification of the optimized crankcase

First, the structural verification of the crankcase in operative conditions has been carried out. Due to the optimisation process, several pockets have been introduced aimed to lighten the component in low-stress areas. The optimisation has been performed with a home-made genetic code based on the generation of fully parametric models generated directly in the Abaqus environment. As design variables, the number of pockets and their dimensions have been chosen. As constraint functions, the maximum allowable stress and the deformation of the component have been set. As objective function (to be minimised) the total mass of the component has been chosen.

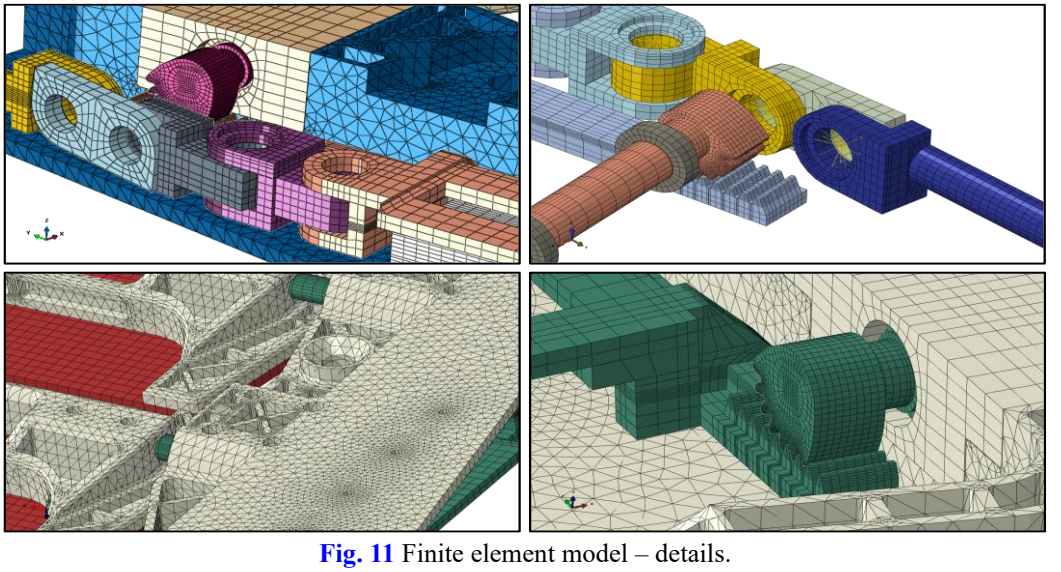

Fig. 11 Finite element model – details.

© Engineered Science Publisher LLC 2023

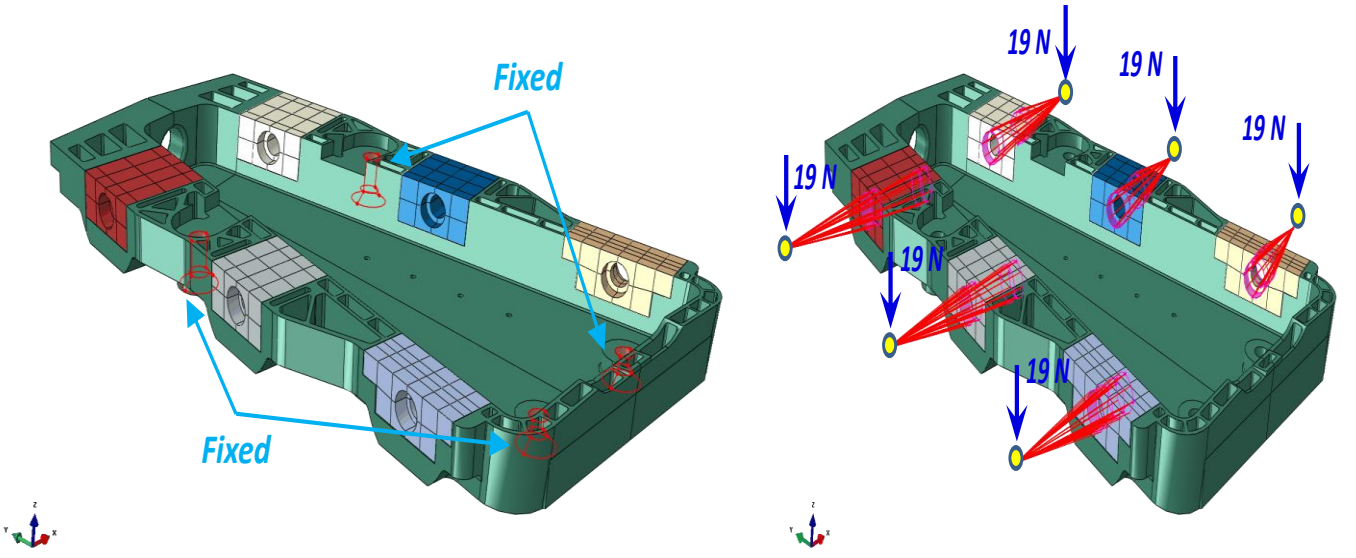

Fig. 12 Analysis 1.1: optimized crankcase - boundary conditions.

It should be noted that the component is not subject to stress of significant intensity, therefore the real minimum weight limit has been imposed by some functional constraints from the manufacturing process and from the coupling with other components.

The load acting on the crankcase component derives from the pressure exerted on the flaps. The pressure load is transferred from the flaps to the gear rods, which are connected to the crankcase. The load has been simulated by means of three RBE2 (Abaqus kinematic coupling). Load (corresponding to 1.9 kg acting on the flaps) is applied on each RBE2 reference node in the Z direction (the most critical one). The crankcase has been fixed at the interfaces with the rear bonnet. A schematization of the adopted boundary conditions is reported in Fig. 12.

The numerical results are reported in Fig. 13 in terms of von-mises stress distribution on the component; while in Table 3, the maximum stress and displacements are reported. The very low values of stresses and displacements, found from this numerical analysis, show that no criticality exist for the optimized crankcase.

Analysis 1.2 – Verification of the optimized side supports

The structural verification of the side supports in operative conditions has, also, been carried out. Fig. 14 shows the boundary conditions applied as for the previous analysis.

The numerical results, in terms of von mises stress distribution, are reported in Fig. 15. In Table 4, maximum stress and displacements for this optimized component are introduced. Also, for this component, no criticalities have been found in terms of maximum stress. Indeed, it can be observed that the maximum stress peaks are negligible (46 MPa) and limited to few localized areas.

Table 3. Analysis 1.1: optimized crankcase - numerically predicted displacements and stresses.

Ux [mm]	Uy [mm]	Uz [mm]	USUM [mm]	von Mises [MPa]
7.45 e-3	2.39 e-3	-2.26 e-2	2.4 e-2	30.8

Table 4. Analysis 1.2: optimized side supports - maximum predicted values.

Ux [mm]	Uy [mm]	Uz [mm]	USUM [mm]	von Mises [MPa]
-7.4 e-3	-6.1 e-3	-2.8 e-2	2.9 e-2	45.9

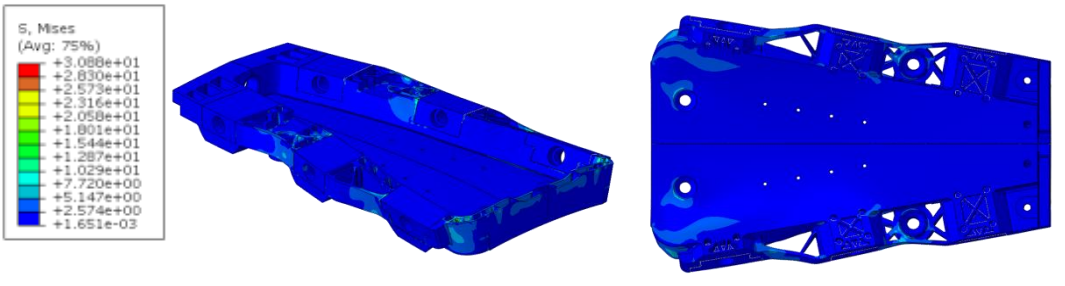

Fig. 13 Analysis 1.1: optimized crankcase - von mises stress distribution.

© Engineered Science Publisher LLC 2023

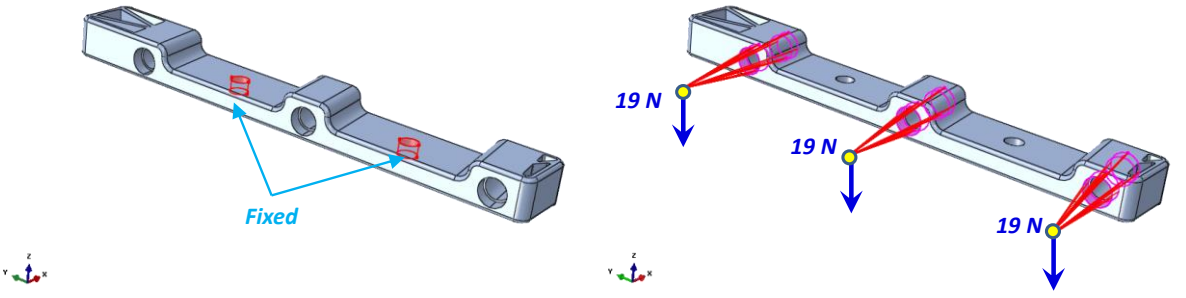

Fig. 14 Analysis 1.2: optimized side supports - boundary conditions.

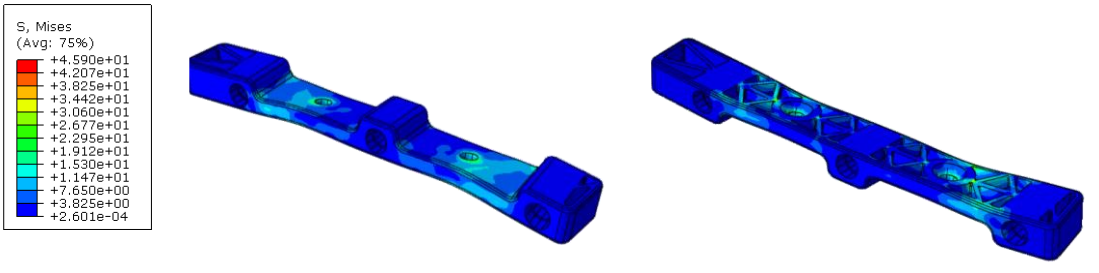

Fig. 15 Analysis 1.2: optimized side supports - von mises stress distribution.

Analysis 1.3 – Verification of the optimized flap supports

The structural verification of the flap supports in operative conditions has been carried out. Fig. 16 shows the boundary conditions (Fig. 16a) and the results in terms of von mises stress (Fig. 16b). The applied 19 N load has been introduced as a uniformly distributed pressure on the flap (0.0018 MPa). In Table 5 the numerical results, in terms of maximum stress and displacements, are presented. According to these results, the maximum stress value is negligible (6.8 MPa) and limited to the connections.

Analysis 2 - Verification of the maximum loading condition in the closed flaps configuration

This analysis was aimed to highlight criticalities in the design of the device, as well as evaluate the stress and deformation

Table 5. Analysis 1.3: optimized flap supports - maximum predicted values.

Ux [mm]	Uy [mm]	Uz [mm]	U_{SUM} [mm]	von Mises [MPa]
-1.0 e-3	-2.1 e-3	-1.2 e-2	1.2 e-2	6.8

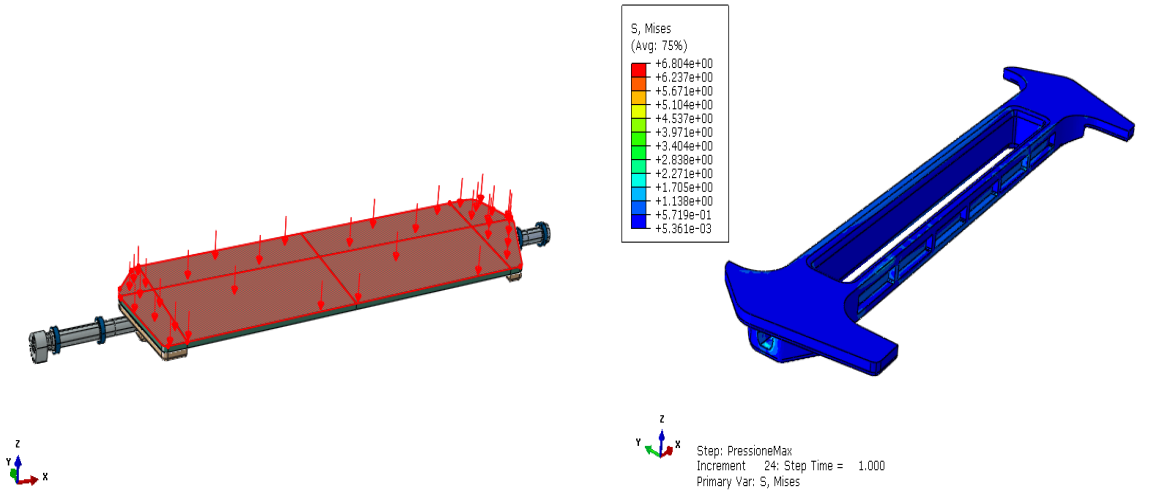

Fig. 16 Analysis 1.2: optimized flap supports - (a) boundary conditions; (b) von Mises stress distribution.

© Engineered Science Publisher LLC 2023

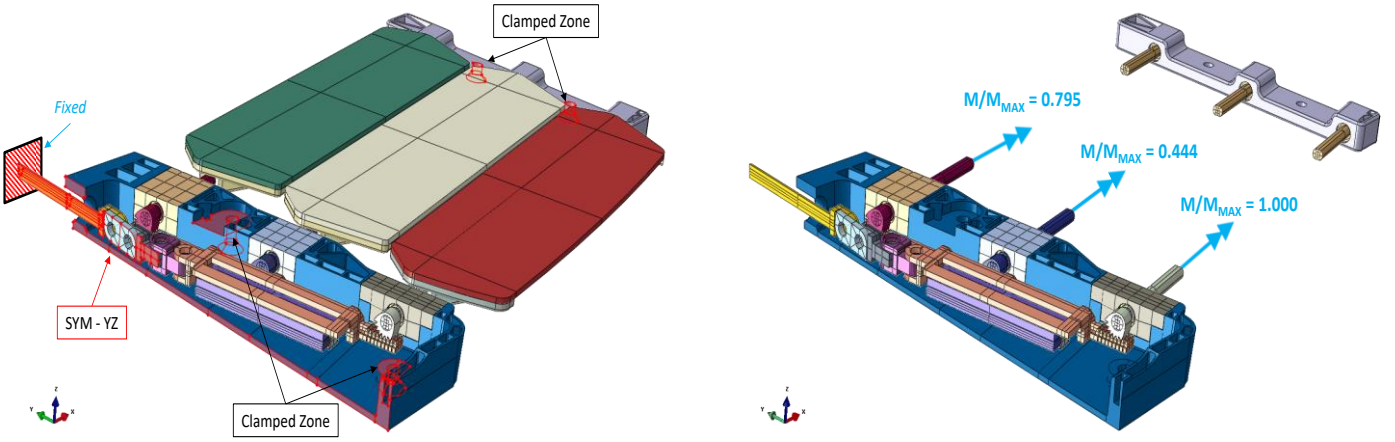

Fig. 17 Analysis 2: Maximum load in closed flaps configuration - boundary conditions.

fields considering the maximum loading condition in the closed flaps configuration. Therefore, Joint 1 (Fig. 9) has been blocked in its non-actuated position and the maximum moments are applied to the edge of the gear rods, as shown in Fig. 17.

According to the obtained numerical results in terms of von mises stress distributions, the higher stresses are reached in the gear/rack contact areas (353 MPa). However, this value derives from the finite element discretization and from a non-uniform contact between the gears and the rack. As a matter of fact, this value drops approximately to 148 MPa in the areas of the rack teeth, by remeshing the areas in contact with the gears. Details of the results in terms of the stress field on the gears and on the racks are reported in Fig. 18.

Table 6 summarises the results of the simulation in terms of maximum stress, maximum displacements, and maximum reaction force, in the longitudinal (Y) direction. Taking into account the symmetry of the model, the total reaction force which should be exerted by the SMA spring to balance the aerodynamic force in closed flap condition is 204 N. Actually, this actuation force falls within the range covered by the chosen SMA springs.

Table 6. Analysis 2: Maximum load in closed flaps configuration - maximum numerically predicted displacements, von mises stress and reaction force.

Ux [mm]	Uy [mm]	Uz [mm]	U_{SUM} [mm]	von Mises [MPa]	Reaction force $R_y/2$ [MPa]
-1.0	-0.75	-0.97	1.013	147	102.0

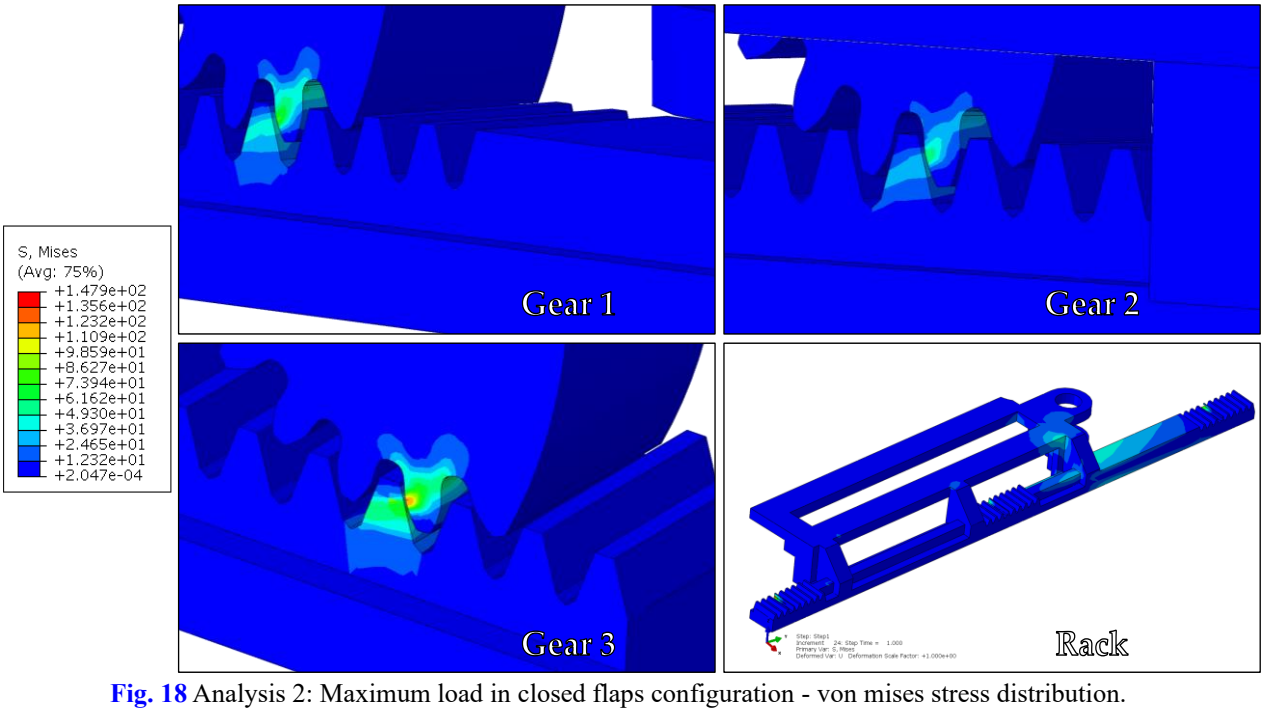

Fig. 18 Analysis 2: Maximum load in closed flaps configuration - von mises stress distribution.

© Engineered Science Publisher LLC 2023

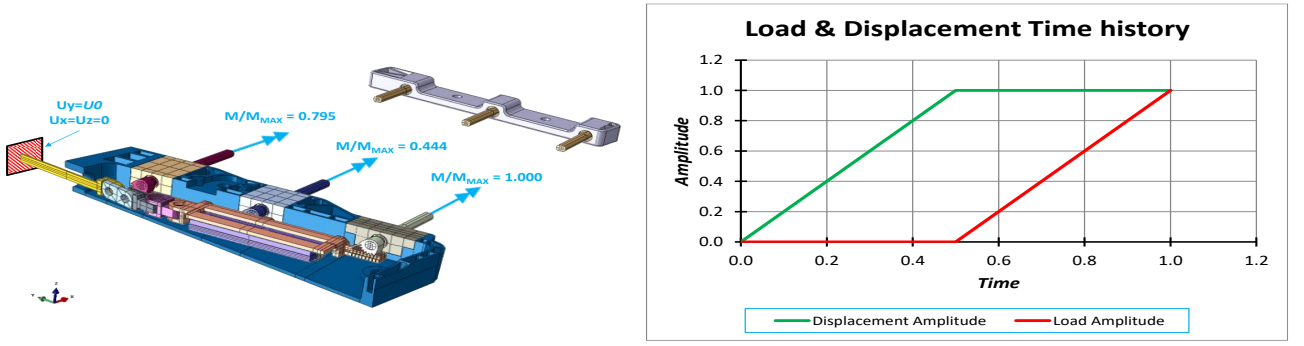

Fig. 19 Analysis 3: Maximum load in opened flaps configuration - (a) boundary conditions; (b) displacement and load amplitudes during the analysis.

Analysis 3 – Verification of the maximum loading condition in the opened flaps configuration

This analysis was aimed to highlight criticalities in the design of the device, as well as evaluate the stress and deformation fields considering the maximum loading condition in the opened flaps configuration. Therefore, Joint 1 (Fig. 9) has been moved and blocked in its actuated position and the maximum moments are applied to the extremities of the gear rods, as shown in Fig. 19a.

This simulation is composed of two consecutive loads steps, as shown in Fig. 19b reporting the load and displacement time histories. Indeed, the imposed displacement is linearly increased from zero up to the maximum value (5mm), which is reached at half the analysis time (0.5), while the moments are kept equal to zero. The 5 mm displacement is then maintained for the remaining part of the simulation, which is completed when the total amount of moment is applied. Therefore, the end of the simulation (time = 1) is characterized by open flap configuration (60° flap rotation and Joint 1 displacement equal to 5 mm) and maximum applied moment.

The evolution during the timestep from the closed to the open flap configuration is shown in Fig. 20 and in Fig. 21, where details of the gear/rack coupling are reported.

According to the obtained numerical results, the stress field up to time = 0.5 is almost zero, since no external load is applied. However, due to the aerodynamic load (time = 1) the stress peaks can be observed in the gear/rack contact areas. Details of the results in terms of the stress field on the gears and on the racks are reported in Fig. 22.

Table 7 summarises the results of the simulation in terms of maximum stress, maximum displacements, and maximum reaction force, in the longitudinal (Y) direction. Taking into

Table 7. Analysis 3: Maximum load in opened flaps configuration - maximum numerically predicted displacements, von mises stress and reaction force.

Ux [mm]	Uy [mm]	Uz [mm]	U_{SUM} [mm]	von Mises [MPa]	Reaction force $R_y/2$ [MPa]
-2.62	-5.5	-27.2	33.5	137	103.2

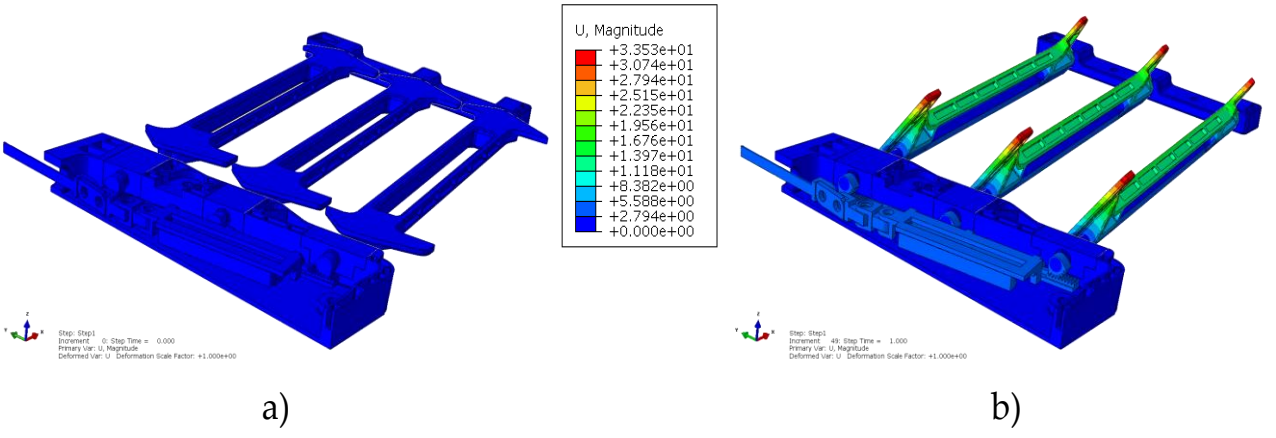

Fig. 20 Analysis 3: Maximum load in opened flaps configuration - (a) displacements in closed flap configuration; (b) displacements in open flap configuration.

 © Engineered Science Publisher LLC 2023

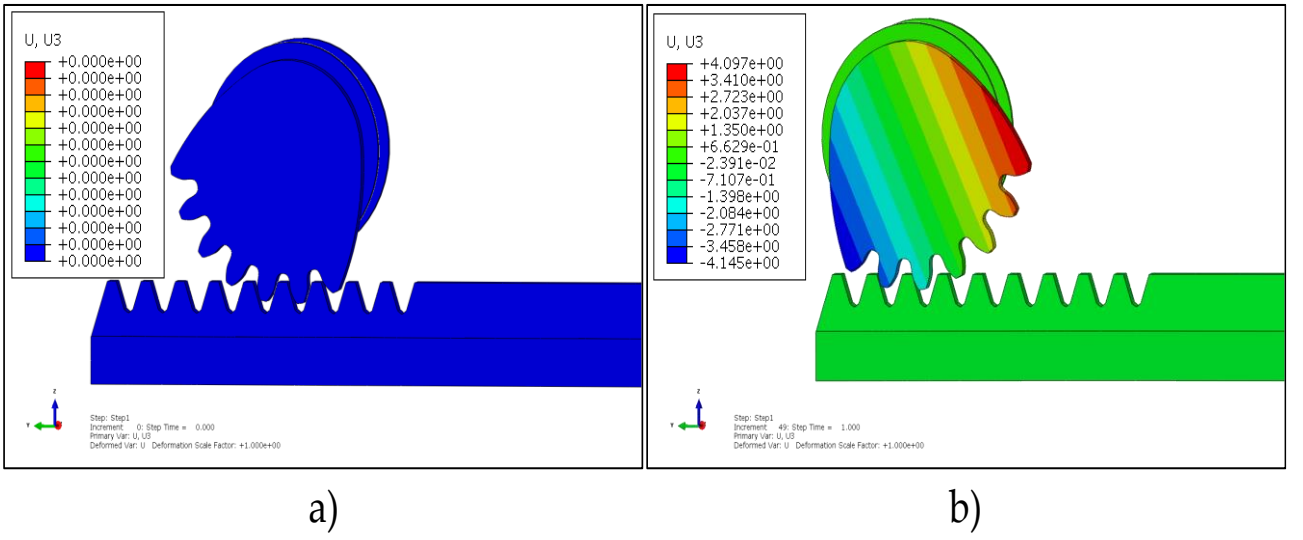

Fig. 21 Analysis 3: Maximum load in opened flaps configuration - Gear/rack detail (a) closed flap configuration; (b) open flap configuration.

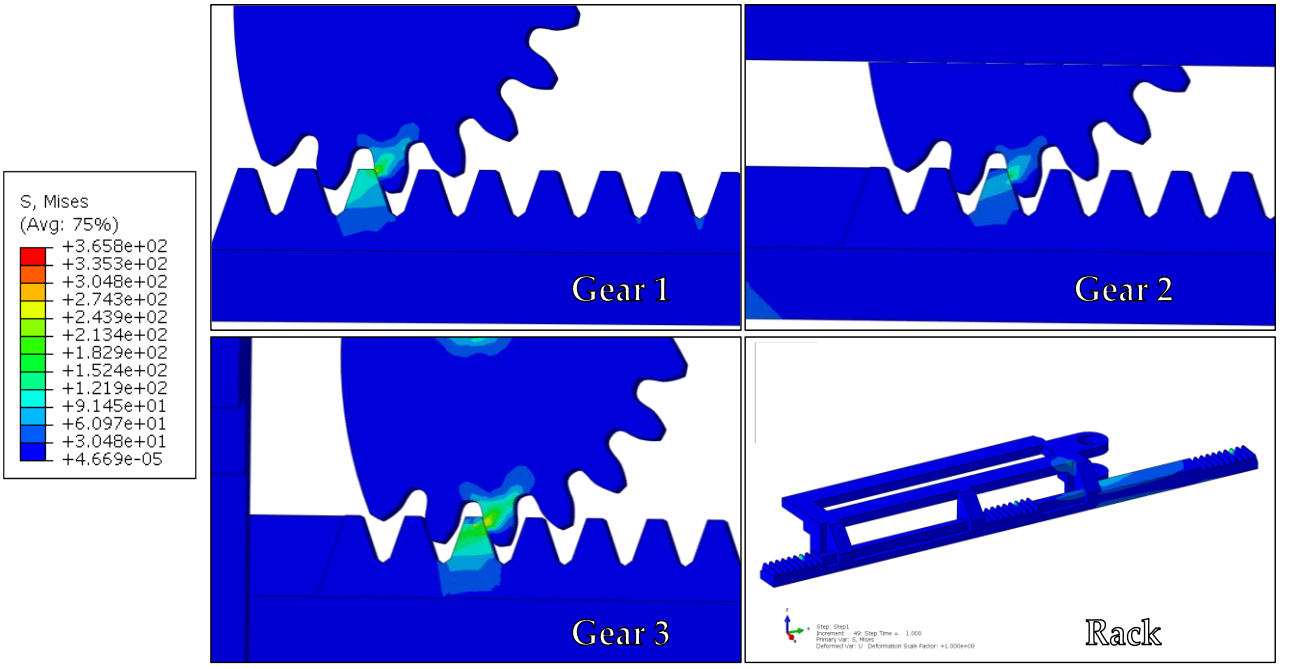

Fig. 22 Analysis 3: Maximum load in opened flaps configuration - von mises stress distribution at the end of the analysis.

account the symmetry of the model, the total reaction force which should be exerted by the SMA spring to balance the aerodynamic force in opened flap condition is. Actually, this actuation force falls within the range covered by the chosen SMA springs

4. Conclusions

In this work, the design verification of a Cooling System Device passively operated by shape memory alloys has been presented. The system is aimed to reduce the temperature inside the engine compartment of a Lamborghini Aventador S vehicle as test case by inducing a 60° rotation of flaps placed on the rear-bonnet of the car. The evolution of the design configurations, due to manufacturing constraints, simplification needs, installation volume and actuation requirements, has been presented and the analyses, performed to verify the presented device under the operating loading conditions, have been introduced. Numerical results have been shown only for the final executive design configurations. Firstly, the effectiveness of the weight optimization phase on the additive manufactured components have been demonstrated. Then the compliance to operational requirements in opened and closed gap configuration has been assessed by evaluating the numerically determined maximum displacements and von Mises stresses under the operating loading conditions.

© Engineered Science Publisher LLC 2023

Conflict of Interest

There is no conflict of interest.

Supporting Information

Not applicable.

References

[1] J. Qiu, C. Wang, C. Huang, H. Ji, Z. Xu, Smart skin and actuators for morphing structures, *Procedia IUTAM*, 2014, **10**, 427-441, doi: 10.1016/j.piutam.2014.01.037.

[2] T. A. Weisshaar, D. K. Duke, Induced drag reduction using aeroelastic tailoring with adaptive control surfaces, *Journal of Aircraft*, 2006, **43**, 157-164, doi: 10.2514/1.12040.

[3] J. Van Humbeeck, Shape memory alloys: a material and a technology, *Advanced Engineering Materials*, 2001, **3**, 837-850, doi: 10.1002/1527-2648(200111)3: 11837: AID-ADEM837>3.0.CO;2-0.

[4] U, Icardi, Ferrero, Preliminary study of an adaptive wing with shape memory alloy torsion actuators, *Materials & Design*, 2009, **30**, 4200-4210, doi: 10.1016/j.matdes.2009.04.045.

[5] D. Coutu, V. Brailovski, P. Terriault, M. Mamou, Y. Mébarki, É. Laurendeau, Lift-to-drag ratio and laminar flow control of a morphing laminar wing in a wind tunnel, *Smart Materials and Structures*, 2011, **20**, 035019, doi: 10.1088/0964-1726/20/3/035019.

[6] J. Manzo, E. Garcia, Demonstration of anin situmorphing hyperelliptical cambered span wing mechanism, *Smart Materials and Structures*, 2010, **19**, 025012, doi: 10.1088/0964-1726/19/2/025012.

[7] M.-L. Dano, M. W. Hyer, SMA-induced snap-through of unsymmetric fiber-reinforced composite laminates, *International Journal of Solids and Structures*, 2003, **40**, 5949-5972, doi: 10.1016/s0020-7683(03)00374-3.

[8] A. Sellitto, A. Riccio, Overview and future advanced engineering applications for morphing surfaces by shape memory alloy materials, *Materials*, 2019, **12**, 708, doi: 10.3390/ma12050708.

[9] W. Wang, H. Rodrigue, S.-H. Ahn, Smart soft composite actuator with shape retention capability using embedded fusible alloy structures, *Composites Part B: Engineering*, 2015, **78**, 507-514, doi: 10.1016/j.compositesb.2015.04.007.

[10] L. Brinson, One-dimensional constitutive behavior of shape memory alloys: thermomechanical derivation with non-constant material functions and redefined martensite internal variable, *Journal of Intelligent Material Systems and Structures*, 1993, **4**, 229-242, doi: 10.1177/1045389X9300400213.

[11] Z. Khoo, J. An, C. Chua, Y. Shen, C. Kuo, Y. Liu, Effect of heat treatment on repetitively scanned SLM NiTi shape memory alloy, *Materials*, 2018, **12**, 77, doi: 10.3390/ma12010077.

[12] J. Mohd Jani, M. Leary, A. Subic, M. A. Gibson, A review of shape memory alloy research, applications and opportunities, *Materials & Design* (1980-2015), 2014, **56**, 1078-1113, doi: 10.1016/j.matdes.2013.11.084.

[13] L. Sun, W. M. Huang, Nature of the multistage transformation in shape memory alloys upon heating, *Metal Science and Heat Treatment*, 2009, **51**, 573-578, doi: 10.1007/s11041-010-9213-x.

[14] I. Mihálcz, Fundamental characteristics and design method for nickel-titanium shape memory alloy, *Periodica Polytechnica Mechanical Engineering*, 2001, **45**, 75-86.

[15] D. C. Lagoudas, Shape memory alloys: modeling and engineering applications (1st ed.), Springer, New York, 2010.

[16] T. Duerig, A. Pelton, D. Stöckel, An overview of nitinol medical applications, *Materials Science and Engineering: A*, 1999, **273-275**, 149-160, doi: 10.1016/s0921-5093(99)00294-4.

[17] L. Sun, W. M. Huang, Z. Ding, Y. Zhao, C. C. Wang, H. Purnawali, C. Tang, Stimulus-responsive shape memory materials: a review, *Materials & Design*, 2012, **33**, 577-640, doi: 10.1016/j.matdes.2011.04.065.

[18] N. B. Morgan, Medical shape memory alloy applications-the market and its products, *Materials Science and Engineering: A*, 2004, **378**, 16-23, doi: 10.1016/j.msea.2003.10.326.

[19] Y. Furuya, Design and material evaluation of shape memory composites, *Journal of Intelligent Material Systems and Structures*, 1996, **7**, 321-330, doi: 10.1177/1045389x9600700313.

[20] D. Stoeckel, Shape memory actuators for automotive applications, *Materials & Design*, 1990, **11**, 302-307, doi: 10.1016/0261-3069(90)90013-a.

[21] C. Bil, K. Massey, E. J. Abdullah, Wing morphing control with shape memory alloy actuators, *Journal of Intelligent Material Systems and Structures*, 2013, **24**, 879-898, doi: 10.1177/1045389x12471866.

[22] D. J. Hartl, D. C. Lagoudas, Aerospace applications of shape memory alloys, Proceedings of the Institution of Mechanical Engineers, *Part G: Journal of Aerospace Engineering*, 2007, **221**, 535-552, doi: 10.1243/09544100jaero211.

[23] A. Vasanthanathan, P. Nagaraj, C. Chandravadhana, N. Vasiraja, Finite element modelling of shape memory alloy based smart link composite satellite structure, *Indian Journal of Structure Engineering*, 2015, **41**, 524-531.

[24] D. H. Mollenhauer, D. M. Thompson, O. Hayden Griffin Jr, Finite element analysis of smart structures, *Advances in Engineering Software*, 1993, **17**, 7-12, doi: 10.1016/0965-9978(93)90036-s.

[25] W.-X. Su, P. Ji, Structural design and finite element verification of auxiliary device for installation of large vertical equipmentShanghai Ligong Daxue Xuebao, *Journal of*

© Engineered Science Publisher LLC 2023

University of Shanghai for Science and Technology, 2011, **33**, 508-510.
[26] J. Cros, P. Viarouge, M. T. Kakhki, Design and optimization of soft magnetic composite machines with finite element methods, *IEEE Transactions on Magnetics*, 2011, **47**, 4384-4390, doi: 10.1109/TMAG.2011.2157113.
[27] A. Riccio, A. Sellitto, D. Borrelli, R. Sansone, A. Caraviello, U. Riccio, A. Torluccio, L. Pacini, R. Mohr, On the development of a passive shape memory alloy- based cooling system–part I: design and implementation, *Engineered Science*, 2023, doi: 10.30919/es927.

Publisher's Note: Engineered Science Publisher remains neutral with regard to jurisdictional claims in published maps and institutional affiliations.

© Engineered Science Publisher LLC 2023